Heliyon 10 (2024) e32278

Contents lists available at ScienceDirect

Heliyon

journal homepage: www.cell.com/heliyon

Research article

Microwave-assisted atmospheric alkaline leaching process and leaching kinetics of rare earth melt electrolysis slag

Yusufujiang Mubula [a], Mingming Yu [a,b,*], Delong Yang [a], Heyue Niu [a], Hongju Gu [a], Tingsheng Qiu [a,b], Guangjun Mei [c]

[a] Jiangxi Provincial Key Laboratory of Low-Carbon Processing and Utilization of Strategic Metal Mineral Resources, Jiangxi University of Science and Technology, Ganzhou, 341000, China
[b] School of Resources and Environmental Engineering, Jiangxi University of Science and Technology, Ganzhou, 341000, China
[c] School of Resources and Environmental Engineering, Wuhan University of Technology, Wuhan, 430070, China

ARTICLE INFO

Keywords:
Rare earth melt electrolysis slag
Microwave-assisted
Atmospheric alkaline leaching
Rare earth elements

ABSTRACT

This study focuses on the difficulty of converting fluorinated rare earth elements into hydroxylated rare earth elements in rare earth melt electrolysis slag (RMES) and proposes the use of a microwave-assisted atmospheric alkaline leaching method for the treatment of RMES. The leaching behavior of RMES under microwave-assisted atmospheric alkaline leaching was studied, and the optimal reaction conditions were determined. Under the conditions of a reaction temperature of 150 °C, initial NaOH concentration of 60 %, NaOH-to-slag mass ratio of 4:1, microwave power of 700 W, reaction time of 120 min, and stirring speed of 300 r/min, the conversion rate of fluorinated rare earths reached 99.17 %. The apparent rate equation of the microwave-assisted atmospheric alkaline leaching process was obtained by leaching kinetic analysis, and the apparent activation energy under this process was calculated to be 54.872 kJ/mol, which was 12.458 kJ/mol lower than that achieved when conventional heating was used for leaching (67.33 kJ/mol).

1. Introduction

Rare earth elements (REEs), which are known as “industrial vitamins” owing to their unique physical and chemical properties, can form a wide variety of new materials with different performance characteristics when combined with other materials. The primary role of these industrial vitamins is to significantly improve the quality and performance of other products [1–4]. Owing to the uneven distribution of primary mineral resources worldwide and the increasing demand for advanced applications, there is a strong emphasis on the development and utilization of rare earth resources; however, this results in large amounts of rare earth solid waste [5]. Current mainstream technology for the molten salt electrolysis of rare earth metals usually utilizes fluorinated molten salts. However, the recovery rate of REEs during molten salt electrolysis is usually less than 95 %, and most of the lost REEs enter the generated rare earth melt electrolysis slag (RMES) [6–8]. As REEs are non-renewable, it is necessary to recycle rare earth solid waste for comprehensive utilization [9], which is crucial for green and sustainable development [10].The key to recovering REEs from RMES is to convert the

* Corresponding author. Jiangxi Provincial Key Laboratory of Low-Carbon Processing and Utilization of Strategic Metal Mineral Resources, Jiangxi University of Science and Technology, Ganzhou, 341000, China.
E-mail addresses: 2585884739@qq.com (Y. Mubula), mingmy1990@163.com (M. Yu), 1261432045@qq.com (D. Yang), 13099525985@163.com (H. Niu), 2512107425@qq.com (H. Gu), qiutingsheng@163.com (T. Qiu), meiguangjun@aliyun.com (G. Mei).

https://doi.org/10.1016/j.heliyon.2024.e32278
Received 5 March 2024; Received in revised form 4 May 2024; Accepted 31 May 2024
Available online 31 May 2024
2405-8440/© 2024 The Authors. Published by Elsevier Ltd. This is an open access article under the CC BY-NC-ND license (http://creativecommons.org/licenses/by-nc-nd/4.0/).

contained rare-earth fluorides into soluble rare earth compounds, which then allows for the leaching extraction of REEs. Tong et al. [11] used a combination of CaO and $Al_2(SO_4)_3$ for co-roasting and activating RMES, which resulted in the conversion of fluorinated REEs into soluble sulfated REEs at 900 °C. Liang et al. [6] mixed silicate and RMES for the roasting and recovery of REEs; after roasting at 850 °C for 1.5 h, the fluorinated REE was transformed into an easily acid-leachable silicated REE and NaF, achieving a rare-earth leaching rate of 99 %. Wu et al. [12] combined sodium carbonate roasting with hydrochloric acid leaching to recover REEs from RMES. The RMES was roasted with sodium carbonate at 700 °C for 2 h, which converted the contained rare-earth fluoride into a rare-earth oxide and achieved a rare-earth leaching rate of 99 %. Lai et al. [13] reconstructed the mineral phase of the RMES by adding $LiOH{\cdot}H_2O$ and combined it with vacuum distillation to recover REEs through subsequent roasting at 600 °C and distillation at 1100 °C. Hu et al. [14] and Wang et al. [15] treated RMES with nitric acid and sulfuric acid calcination, respectively, and successfully converted fluorinated REEs into soluble nitric acid/sulfuric acid REEs at around 250 °C at a conversion rate of >95 %. Yang et al. [16] mixed 80 % concentrated NaOH solution with RMES and achieved a leaching efficiency of REEs of up to 99 % within a reaction time of 3 h at 200 °C. Although the aforementioned methods can achieve relatively high REE leaching rates, they suffer from high reaction temperatures and excessive concentrations of chemical agents, which result in the consumption of large amounts of energy and chemicals. In addition, these high-temperature reactions generate toxic and harmful gases that lead to environmental pollution. Therefore, there is an urgent need for a green and efficient extraction method to recover Rees. In recent years, many researchers have applied microwave heating technology to hydrometallurgical leaching processes to improve the leaching rate of useful metals, shorten the leaching reaction time, and reduce energy consumption [17]. The heating principles of microwave heating and conventional heating are completely different; while conventional heating involves heat conduction, microwave heating involves the direct transfer of energy via selective heating, which conventional heating cannot provide [18]. Microwaves are widely used in the fields of thermal decomposition, thermal drying, pyrometallurgy, and hydrometallurgy leaching [19,20]. Wen et al. [21,22] studied the microwave-assisted leaching of copper from chalcopyrite and found that microwave heating could increase the boiling point of the leaching system and promote the leaching of copper by changing the surface structure of the chalcopyrite and reducing the passivation layer. Thomas et al. [23] utilized microwave-assisted hydrometallurgical leaching to recover elements such as platinum, rhodium, and cerium from spent catalysts without requiring the pretreatment of materials or addition of oxidants. Laubertova et al. [24] showed that microwave-assisted leaching can increase the reaction rate by more than two times during the recovery of Zn and Pb from arc-furnace dust. Wang et al. [25] found that microwave heating significantly reduced the activation energy of vanadium during the reaction process. Huang et al. [26] investigated the microwave-assisted leaching behavior of a mixed rare-earth concentrate, and found that the REE leaching rate was 16.49 % higher than that achieved by the traditional leaching method. In the above process, microwave thermal decomposition occurs during the heating process, causing the structure of the material to be destroyed with low energy consumption and no pollution; such thermal decomposition of minerals has a wide range of application prospects [27]. Owing to these advantages in regards to reduction in the amount of chemicals and energy consumed, microwave heating was used in this study to treat the RMES to convert the physical phase. In addition, the influence of the experimental conditions on the conversion of fluorinated REEs to hydroxylated REEs was investigated, and the leaching kinetics of the fluorinated REE conversion process were analyzed.

2. Materials and methods

2.1. Raw materials

The RMES used in this experiment was provided by a company in Jiangxi, China. The raw material was ground to 200 mesh (<74 μm) prior to the experiments. The chemical composition was characterized using inductively coupled plasma emission spectroscopy (ICP) and atomic absorption spectroscopy (AAS). As shown in Table 1, the atomic composition of RMES was 44.68 % Nd, 12.46 % Pr, 33.51 % F, 3.62 % Li, 0.93 % Ca, and 0.25 % Al, with the primary REEs being Nd and Pr. X-ray diffraction (XRD) analysis revealed that the main components of the RMES were NdF_3, PrF_3, PrOF, and LiF (Fig. 1).

2.2. Experimental method

First, a certain amount of RMES and a certain concentration of NaOH solution were placed in a polytetrafluoroethylene (PTFE) flask, which was heated to the experimental temperature in a microwave oven while under stirring by a magnetic stirring rotor; the reaction equipment and process are shown in Fig. 2. After the reaction was complete, the products were washed with deionized water and the alkaline leaching residue was filtered and dried for solid–liquid separation. Then, the conversion rate of fluorinated REEs to hydroxylated REEs was analyzed by performing quantitative and qualitative analyses on the leaching slag through XRD. Additionally, the content of F in the aqueous washing solution was detected as an index of the reaction efficiency using equations (1) and (2) as follows: the effects of the initial NaOH concentration, NaOH-to-slag mass ratio, microwave power, reaction temperature, reaction time, and stirring speed on the conversion rate of the fluorinated REEs were investigated.

Table 1
Composition of RMES (wt%).

Element	Nd	Pr	F	Li	Ca	Al	Other
Content (%)	44.68	12.46	33.51	3.62	0.93	0.25	4.55

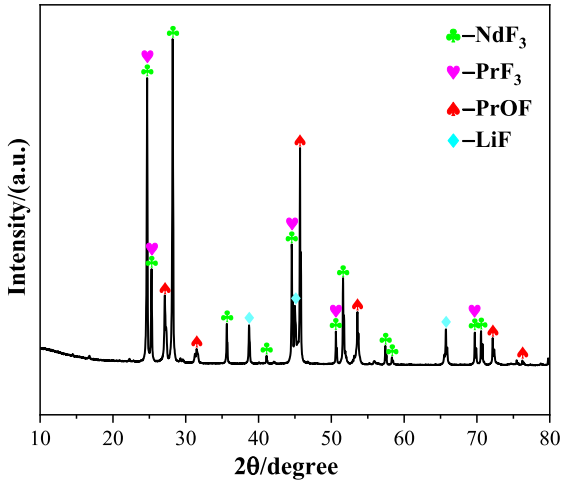

Fig. 1. XRD pattern of RMES.

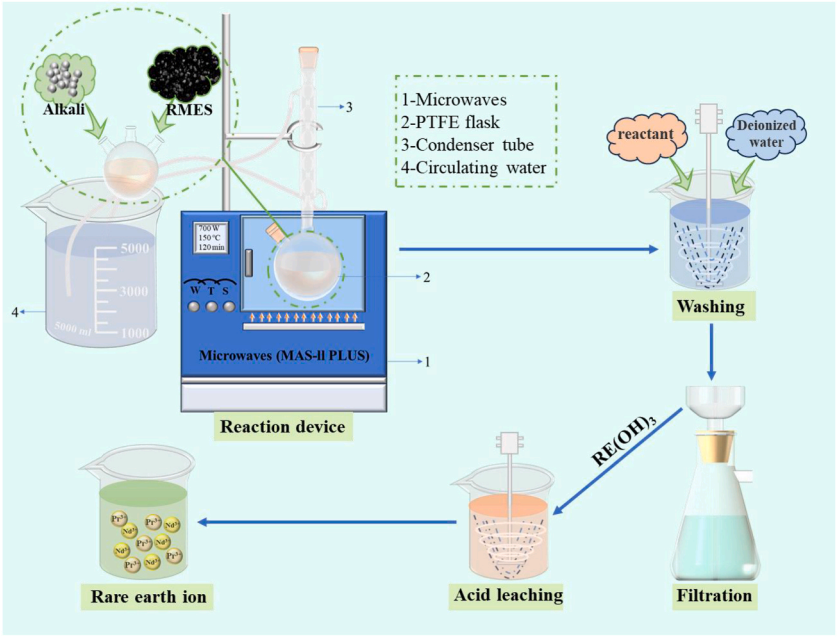

Fig. 2. Reaction equipment and process.

$$\text{Conversion rate}: \eta = \left(1 - \frac{M \cdot W}{M_0 \cdot W_0}\right) \times 100\% \tag{1}$$

$$\text{Leaching rate}: \eta = \frac{C \cdot V}{M_0 \cdot W_0} \times 100\% \tag{2}$$

In Eqs. (1) and (2), M represents the mass of the reaction product after alkaline leaching (g), W represents the mass fraction of fluorinated REEs in the alkaline leaching products (wt %), C represents the concentration of F in the aqueous washing solution (g/L), V represents the volume of the leaching solution (L), M_0 represents the mass of RMES used in the alkaline leaching process (g), and W_0 represents the initial mass fraction of fluorinated REEs in the RMES used in the alkaline leaching process (wt %).

2.3. Equipment and reagent

A physical phase analysis of the raw materials and reaction products was performed using an X-ray diffractometer (Ultima IV, Rigaku, Japan). The raw materials and reaction products were analyzed using scanning electron microscopy (SEM; MLA650F, FEI, USA), energy-dispersive X-ray spectroscopy (EDS; MLA650F, FEI, USA), X-ray photoelectron spectroscopy (XPS; PHI5000VersaProbe, Japan) The chemical composition was characterized using inductively coupled plasma emission spectroscopy (ICP; HORIBA, Ultima2), atomic absorption spectroscopy (AAS; GGX-600, Hai Guang, China), microwaves (MAS-ll PLUS, China), and ion chromatography (IC; Thermo Scientific Integrion ICS-900, America). Sodium hydroxide (XIHUA, China) was used as the primary chemical reagent.

3. Results and discussion

3.1. Comparison of microwave-heated leaching with conventional leaching

To study the differences between microwave-heated leaching and conventional leaching, the effects of the two methods on the alkali conversion of fluorinated REEs were analyzed. The leaching rate of F from fluorinated REEs was measured under the same experimental conditions: reaction temperature of 110–160 °C, microwave heating power of 700 W, initial NaOH concentration of 60 %, NaOH-to-slag mass ratio of 4:1, and stirring speed of 300 r/min. Conventional heating for alkali conversion was performed in an oil-bath heating kettle. As can be seen from Fig. 3, the leaching rate of F from the fluorinated REEs gradually increased with increasing reaction time for both methods, reaching a maximum value of 99.17 % at 150 °C at 120 min for microwave heating (Fig. 3(a)) and a maximum value of 99.08 % at 150 °C at 160 min for conventional heating (Fig. 3(b)). Therefore, it was found that under the same conditions, the leaching rate of F from fluorinated REEs was significantly improved by microwave heating compared to conventional heating. Furthermore, at the selected optimal reaction time of 120 min, the difference in the leaching rate of F was 17.06 %.

3.2. Effect of reaction factors on the phase transition of fluorinated REEs during microwave heating process

In this study, the conversion rate of fluorinated REEs into hydroxylated REEs was measured, and the effects of the microwave heating reaction temperature, initial NaOH concentration, microwave power, NaOH-to-slag mass ratio, and stirring speed on the conversion rate were investigated to determine the optimal reaction conditions.

3.2.1. Effect of temperature on the conversion of fluorinated REEs

To investigate the effect of reaction temperature on the conversion of fluorinated rare earth phases, the temperature was varied between 110 and 160 °C. As shown in Fig. 4, the conversion of NdF_3, PrF_3 and PrOF in the fluorinated REEs increased from 22.77 % to 21.49 %–99.21 % and 99.11 %, respectively, as the temperature increased from 110 °C to 150 °C. This is because the increase in temperature was favorable for the diffusion of NaOH in the reactant slurry and the kinematic activity of the fluorinated rare-earth molecules, which then led to better contact between the reactants and the alkali medium, thus improving the conversion efficiency. However, when the temperature exceeded 150 °C, the conversion rate of the fluorinated REEs increased slowly. Therefore, 150 °C was selected as the optimum reaction temperature.

3.2.2. Effect of initial NaOH concentration on the conversion of fluorinated REEs

The effect of the initial NaOH concentration (30–80 %) on the phase conversion of the fluorinated REEs was investigated. As shown in Fig. 5, the conversion of NdF_3,PrF_3 and PrOF in the fluorinated REEs increased from 31.92 % to 30.16 %–99.15 % and 99.12 %, respectively, when the initial NaOH concentration was increased from 30 % to 60 %; this was attributed to the increase in NaOH concentration facilitating a higher mass-transfer efficiency between the solid and liquid interfaces, which in turn increased the conversion of the fluorinated REEs. However, when the initial concentration exceeded 60 %, there was no obvious increase in the conversion rate of the fluorinated REEs. Therefore, 60 % was selected as the optimal initial concentration.

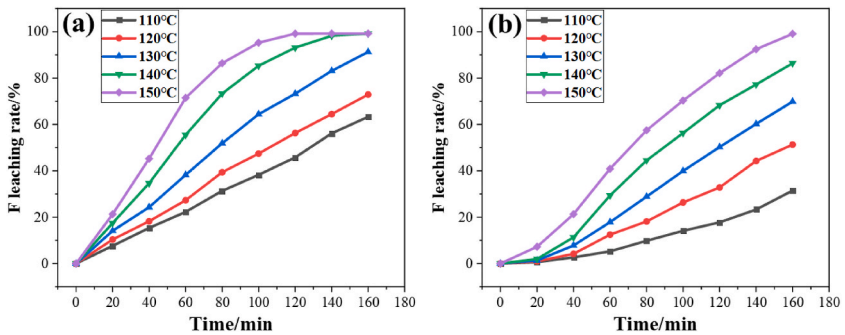

Fig. 3. Leaching rate of element F in fluorinated rare earths(a) microwave heating conditions; (b) conventional heating conditions.

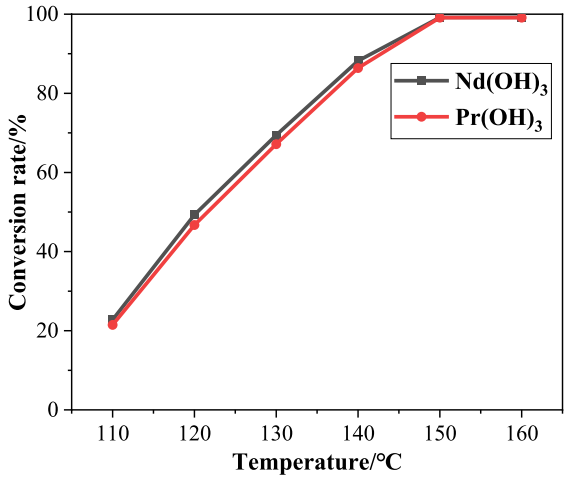

Fig. 4. Effect of temperature on the conversion of fluorinated rare earths (NaOH initial concentration:60 %, NaOH-slag mass ratios 4:1, microwave power: 700W, stirring speed: 300r/min, time: 120min).

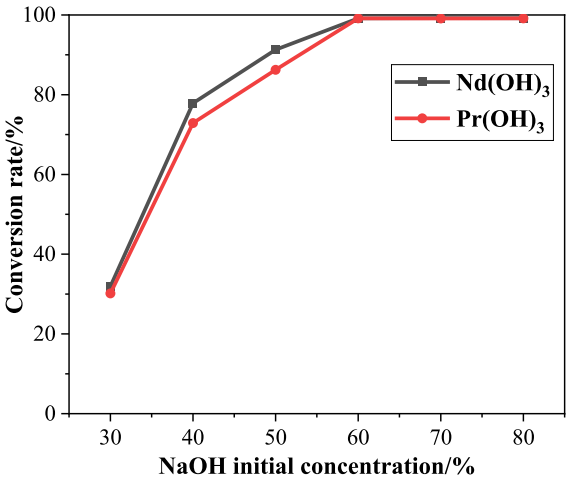

Fig. 5. Effect of NaOH initial concentration on the conversion of fluorinated rare earths (temperature: 150 °C, NaOH-slag mass ratios 4:1, microwave power: 700W, stirring speed: 300r/min, time: 120min).

3.2.3. Effect of NaOH-to-slag mass ratio on the conversion of fluorinated REEs

The effect of the NaOH-to-slag mass ratio (2:1–6:1) on the physical phase reconstruction of fluorinated REEs was investigated. As shown in Fig. 6, the conversion rates of NdF_3,PrF_3 and PrOF in fluorinated REEs increased from 34.24 % to 31.46 %–99.21 % and 99.07 %, respectively, when the NaOH-to-slag mass ratio was increased from 2:1 to 4:1. This is because an increase in the NaOH-to-slag mass ratio was conducive to the enhancement of the overall wave absorbance of the reactant slurry, such that the energy transmitted by the microwave to the reactant slurry was better transformed into reaction heat energy, thereby improving the conversion rate of the fluorinated REEs. However, when the NaOH-to-slag mass ratio was higher than 4:1, the conversion rate of the fluorinated REEs decreased. This decline was attributed to the viscosity of the slurry increasing with the NaOH mass ratio, which limited the transfer activity of the reactants and media in the reaction system and led to a lower probability of contact between the alkali and slag. Therefore, 4:1 was identified as the optimal NaOH-to-slag mass ratio.

3.2.4. Effect of microwave power on the conversion of fluorinated REEs

To study the effect of microwave power on the conversion of fluorinated REEs in the physical phase, the microwave power was varied between 300 and 900 W. As can be seen from Fig. 7, when the microwave power was increased from 300 W to 700 W, the conversion rates of NdF_3,PrF_3 and PrOF in the fluorinated REEs increased from 83.23 % to 81.11 %–99.21 % and 99.09 %, respectively. This is because, as the microwave power increased, more energy was transmitted to the reactant slurry per unit time, which resulted in rapid heating of the reactant slurry and provided abundant energy to impart highly active movement to the ions in the reactant slurry,

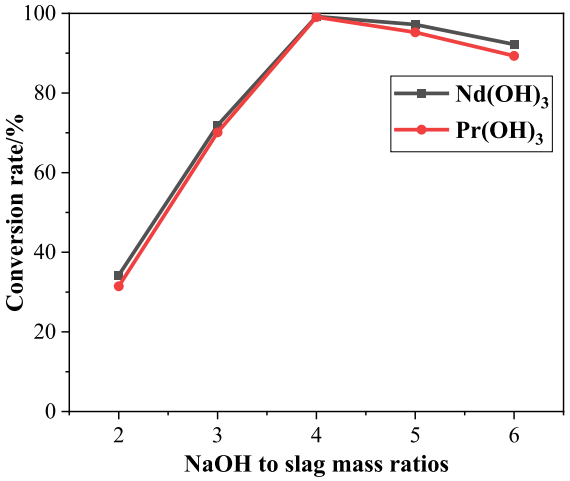

Fig. 6. Effect of NaOH to slag mass ratios on the conversion of fluorinated rare earths (temperature: 150 °C, NaOH initial concentration:60 %, microwave power: 700W, stirring speed: 300r/min, time: 120min).

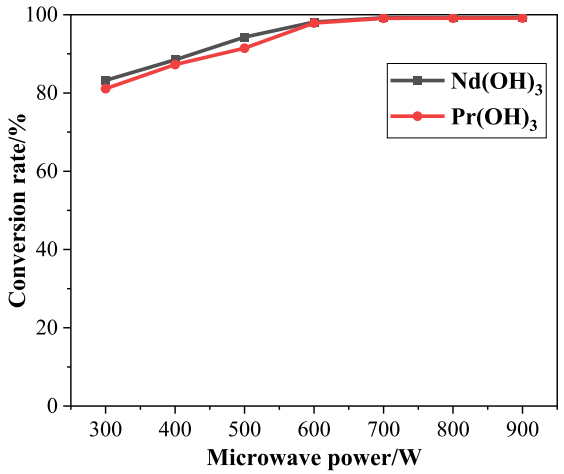

Fig. 7. Effect of microwave power on the conversion of fluorinated rare earths (temperature: 150 °C, NaOH initial concentration:60 %, NaOH to slag mass ratios:4:1, stirring speed: 300r/min, time: 120min).

thus improving the reaction rate. When the microwave power exceeded 700 W, the conversion rate of the fluorinated REEs did not increase significantly; therefore, 700 W was selected as the optimal microwave power.

3.2.5. Effect of stirring speed on the conversion of fluorinated REEs

The effect of stirring speed (0–500 r/min) on the phase conversion of fluorinated REEs was investigated. As can be seen from Fig. 8, when the stirring speed was increased from 0 r/min to 300 r/min, the conversion of NdF_3,PrF_3 and PrOF in the fluorinated REEs increased from 31.44 % to 30.36 %–99.17 % and 99.11 %, respectively. This may be due to the high concentration of the leaching system causing stratification when stirring did not occur, which was not conducive to the reaction. Using the appropriate stirring speed aided in establishing full contact between the reactants, alkaline medium, and intermediates in the electrolyte, which caused the reaction to proceed more thoroughly. However, when the stirring speed exceeded 300 rpm, the conversion rates of Nd and Pr in the fluorinated REEs decreased with increasing stirring speed. This is because the minerals rotated with the alkaline medium when the speed was too high, forming a relatively static state, which reduced the probability of contact and affected mass transfer effect on the suspension; thus, 300 rpm was selected as the optimal stirring speed.

3.3. Conversion process of fluorinated REEs

To investigate the phase conversion process of fluorinated REEs into hydroxylated REEs under microwave heating conditions, raw ore samples and reaction products were analyzed using SEM, EDS, XRD, and XPS.

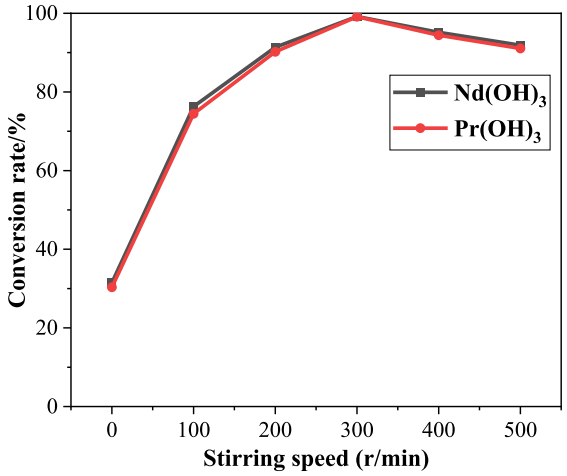

Fig. 8. Effect of stirring speed on the conversion of fluorinated rare earths (temperature: 150 °C, NaOH initial concentration:60 %, NaOH to slag mass ratios:4:1, microwave power: 700W, time: 120min).

The XRD (Fig. 1), SEM, and EDS patterns (Fig. 9 (a)) of the raw ore showed that the fluorinated REEs in the RMES were mainly NdF_3,PrF_3 and PrOF, containing 38.02 % F, and their surface morphology comprised irregular and smooth tiny particles. Fig. 9 shows the SEM images and EDS spectra and Fig. 10 shows the XRD patterns of the reaction products obtained under the following reaction conditions: reaction temperature of 110–150 °C, microwave power of 700 W, reaction time of 2 h, stirring speed of 300 rpm, and NaOH-to-slag mass ratio of 4:1. When the microwave heating temperature was 110 °C, the surface of the ore sample began to be damaged—the smooth morphology of the original surface transformed to a rougher morphology—and the content of F decreased, as shown by the SEM image and EDS spectrum, respectively (Fig. 9(b)). Furthermore, Fig. 10 shows that the NdF_3, PrF_3 and PrOF peaks gradually weakened, and $Nd(OH)_3$ and $Pr(OH)_3$ peaks began to appear, indicating that the fluorinated REEs began to be converted into hydroxylated REEs at 110 °C. The EDS results confirmed that the fluorinated REEs were transformed into hydroxylated REEs. When the microwave heating temperature was 120 °C, there were many holes and cracks on the surface of the ore sample and the F content decreased from the original 38.02 %–18.77 % (Fig. 9(c)); furthermore, XRD (Fig. 10) showed that the peaks of $Nd(OH)_3$ and $Pr(OH)_3$ increased in intensity while the peaks of NdF_3,PrF_3 and PrOF weakened gradually. When the microwave heating temperature was 130 °C, the ore sample began to significantly decompose and the presence of tiny crystals attached to the surface of the damaged rough particles could be observed (Fig. 9(d)). Furthermore, EDS showed that the content of F decreased to 11.97 % (Fig. 9(d)). XRD (Fig. 10) showed that a large number of obvious $Nd(OH)_3$ and $Pr(OH)_3$ peaks appeared on the spectra. Simultaneously, a small number of characteristic peaks of NdF_3, PrF_3 and PrOF were detected. When the microwave heating temperature was 140 °C, the mineral samples, except for some small particles, had transformed into small crystal particles in the form of agglomerates (Fig. 9(e)); furthermore, the F content decreased to 6.17 % (Fig. 9(e)). Meanwhile, the XRD pattern (Fig. 10) mainly comprised peaks corresponding to $Nd(OH)_3$ and $Pr(OH)_3$, and the characteristic peaks of NdF_3, PrF_3 and PrOF were not detected. When the microwave heating temperature was 150 °C, the mineral samples had all turned into small-grained crystals, and the F content decreased from the original 38.02 to 0 % (Fig. 9(f)). The XRD pattern (Fig. 10) mainly comprised peaks corresponding to $Nd(OH)_3$ and $Pr(OH)_3$, and the characteristic peaks of NdF_3, PrF_3 and PrOF were not detected. This indicates that the fluorinated REEs in the raw material were almost completely converted into hydroxylated REEs. In addition, the SEM morphologies showed that increasing the reaction temperature resulted in an increasing degree of cracks on the surfaces of the mineral samples, which increased the specific surface areas of the minerals. This may be due to the fact that the microwave energy transferred thermal energy through the reaction system, which comprised a specific ratio of mineral samples and alkali medium; due to the inhomogeneity of the microwave action, a temperature difference was generated, which in turn generated thermal stresses, which increased the specific surface areas of the reactant mineral samples.

The XPS spectra of the original sample and reaction product (Fig. 11(a)) show obvious F peaks in four places, and that the relative atomic composition of F atoms was the highest at 78.1 %; this was due to the chemical bonding in the original samples of NdF_3,PrF_3 and PrOF mainly being the ionic bonding between F and the REEs, resulting in the composition of the rest of the elemental atoms being lower and their peaks being weaker. Fig. 11(b) shows that the F peak disappeared, resulting in there only being one weak peak at a binding energy of 682.4 eV, and the relative atomic composition of F reduced to 1.2 %. In addition, the relative composition of O atoms was the highest at 81.7 %, and a new Nd peak was observed; furthermore, the relative compositions of Nd and Pr atoms also increased from 7.7 % to 1.7 %–14.2 % and 2.9 %, respectively, because NdF_3,PrF_3 and PrOF in the pristine samples were almost completely converted to $Nd(OH)_3$ and $Pr(OH)_3$. After the microwave heating reaction, under the dual action of mineral decomposition conversion and the temperature difference generated by the microwaves, the specific surface areas of the minerals gradually increased with increasing temperature, which resulted in the formation of rough cracks and/or pore structures on the originally smooth surfaces of the mineral sample particles. This made the minerals looser and easier to decompose and transform, which was conducive to the subsequent reaction proceeding more thoroughly. In this process, as the reaction proceeded, the mineral surface continued to decompose and change in structure, while the chemical bonding also changed from ionic bonding between F and the REEs to chemical bonding

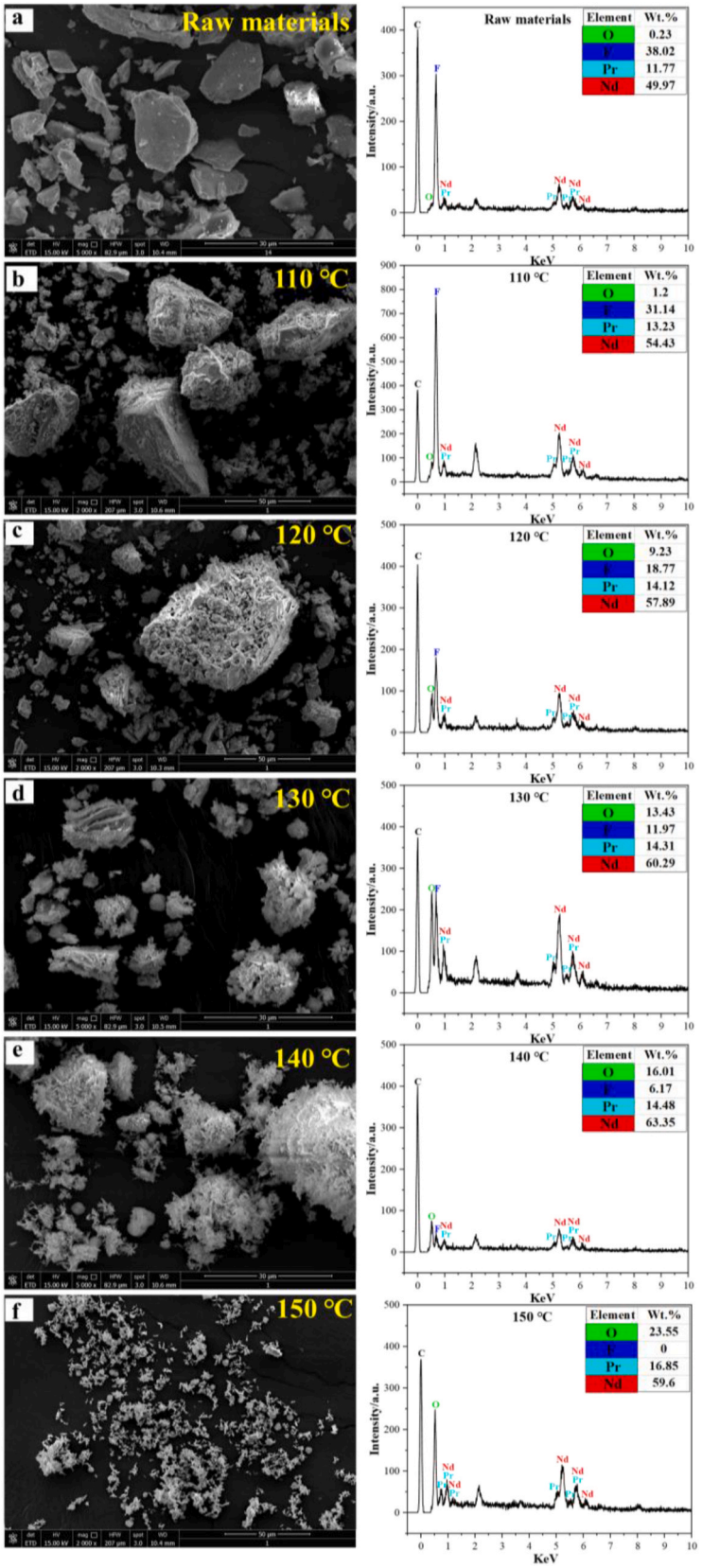

(caption on next page)

Fig. 9. SEM and EDS pattern of (a) raw RMES; (b–f) the reaction products at different temperature (110–150 °C), reaction time of 120 min, stirring speed of 300 r/min, NaOH to slag mass ratios of 4:1, NaOH initial concentration of 60 % and microwave power of 700W

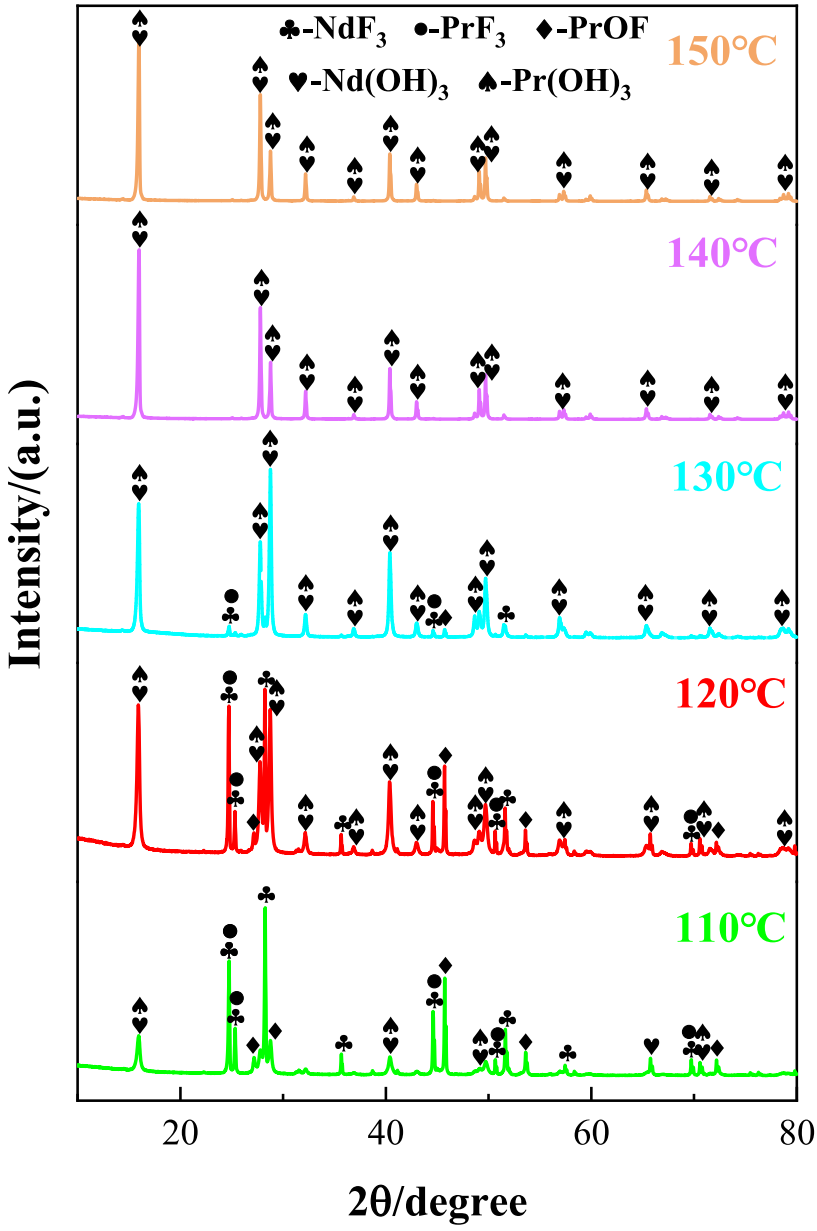

Fig. 10. XRD pattern of the reaction products at different temperature (110–150 °C), reaction time of 120 min, stirring speed of 300 r/min, NaOH to slag mass ratios of 4:1, NaOH initial concentration of 60 % and microwave power of 700W

between –OH and the REEs. Thus, the microwave heating process successfully realized the decomposition conversion of fluorinated REEs into hydroxylated REEs, which guaranteed their subsequent leaching and recovery.

3.4. Leaching kinetics of alkaline leaching process

To further analyze the conversion process of fluorinated REEs during the microwave heating reaction, the classical "unreacted nucleus contraction model" was used to analyze the leaching kinetics of the conversion process. Hydroxylated REEs and NaF were produced during the conversion of fluorinated REEs and fluorinated rare-earth oxides, according to the reaction equations (3)–(6); this is essentially a solid–liquid reaction, and the reaction behavior can be described by the unreacted nucleus contraction model [28].

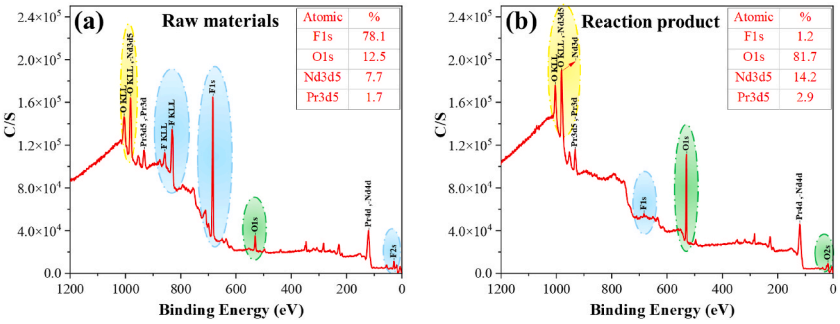

Fig. 11. XPS pattern of (a) raw RMES; (b) the reaction products at reaction temperature of 150 °C, reaction time of 120 min, stirring speed of 300 r/min, NaOH to slag mass ratios of 4:1, NaOH initial concentration of 60 % and microwave power of 700W

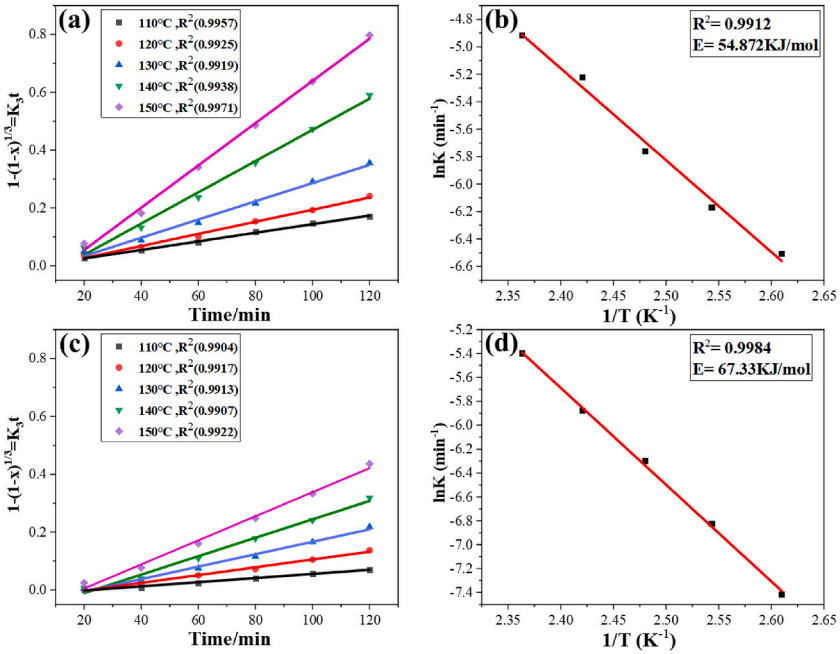

Fig. 12. Plots of $1-(1-X)^{1/3} = K_3t$ of (a) microwave heating conditions, (b) microwave heating conditions Arrhenius plots of F-element leaching from fluorinated rare earths; (c) conventional heating conditions,(d) conventional heating conditions Arrhenius plots of F-element leaching from fluorinated rare earths.

According to this model, the reaction rate between solid particles and the reacting reagent can be controlled by one of the following steps: diffusion through the product layer, diffusion through the fluid film, or chemical reactions at the particle surface [29–31]. The integral rate equations for these models can be expressed as $1 + 2(1-X) - 3(1-X)^{2/3} = K_1t$, $1-(1-X)^{2/3} = K_2t$, $1-(1-X)^{1/3} = K_3t$,where X is the rate of leaching of F from the fluorinated REEs, t is the reaction time, K_1 is the rate constant for pore diffusion, K_2 is the apparent rate constant for diffusion through the fluid film, and K_3 is the apparent rate constant for surface chemical reactions.

$$NdF_3 + 3NaOH = Nd(OH)_3 + 3NaF \quad (3)$$

$$PrF_3 + 3NaOH = Pr(OH)_3 + 3NaF \quad (4)$$

$$PrOF + NaOH + H_2O = Pr(OH)_3 + NaF \quad (5)$$

$$Li + NaOH = LiOH + NaF \quad (6)$$

To determine the rate-limiting step of the kinetic reaction of the fluorinated REE conversion process, the leaching rate data of F from the fluorinated REEs (Fig. 3) were used in calculations with the above model equations and evaluated by linear fitting; the results are shown in Fig. 12(a–c). The kinetic equation $1-(1-X)^{1/3} = K_3t$ was an appropriate fit for the leaching rates of F from fluorinated REEs obtained via the microwave and conventional heating methods under different temperature conditions; the correlation coefficient R^2 was above 0.99, owing to which the best linear relationship obtained was$1-(1-X)^{1/3} = K_3t$. Based on these results, a kinetic

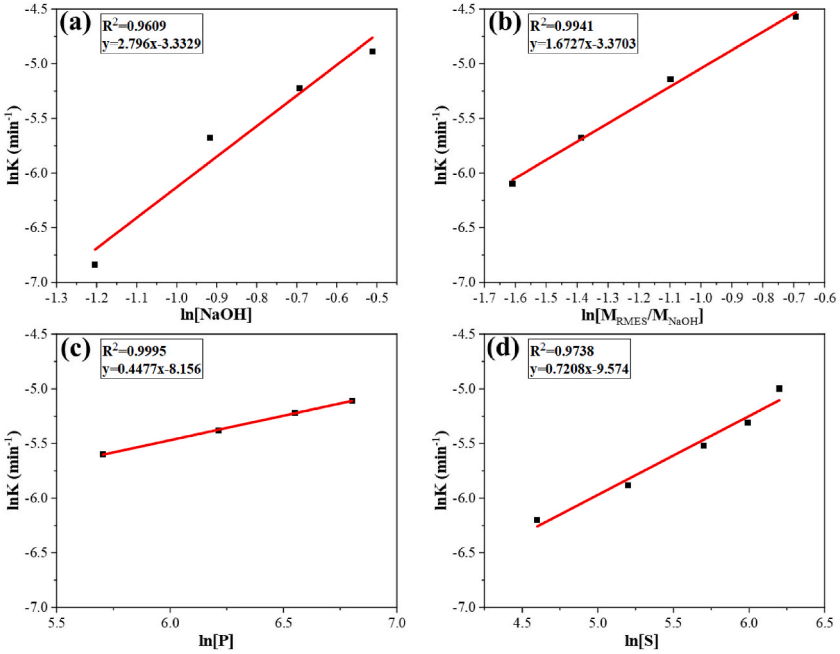

Fig. 13. Microwave heating conditions Arrhenius plots of F-element leaching from fluorinated rare earths (a) NaOH initial concentration; (b) NaOH to slag mass ratios; (c) microwave power; (d) stirring speed.

equation for the process that obeys the chemical reaction on the surface was determined.

As shown in Fig. 12(a–c), the slopes of the fitted straight lines were linearly fitted to ln K versus 1/T according to the Arrhenius equation $K = Ae^{-E/RT}$ to obtain the Arrhenius curves of the reaction rate constants versus temperature for the conversion of fluorinated REEs to rare earth compounds under both the microwave and conventional heating processes (Fig. 12(b–d)). The apparent activation energy for the conversion of fluorinated REEs to rare-earth compounds was calculated to be E = 54.872 kJ/mol during the microwave heating process and E = 67.33 kJ/mol during the conventional heating process; the apparent activation energy of the microwave heating method was 12.458 kJ/mol lower than that of the conventional heating method, indicating that the microwave heating method effectively reduced the apparent activation energy. Using the above method, the linear fitting curves of ln k versus ln[NaOH], $\ln[M_{RMES}/M_{NaOH}]$, ln[P], and ln[S] were obtained using Eqs. for the initial NaOH concentration, alkali residue ratio, microwave power, and stirring speed, respectively (Fig. 13). The slopes of the fitting curves of the reaction rate constant k with the reaction temperature, reaction time, initial NaOH concentration, alkali residue ratio, microwave power, and stirring speed corresponded to the reaction levels of the factors in the microkinetic equation for the conversion of fluorinated REEs to rare-earth compounds. Thus, the microkinetic equation of the above microwave-enhanced conversion process can be described as follows:

$$1-(1-X)^{1/3} = 56.38[NaOH]^{2.796}[M_{RMES}/M_{NaOH}]^{1.6727}[P]^{0.4477}[S]^{0.7208}e^{-54872t/RT}$$

4. Conclusion

(1) After the microwave-assisted atmospheric alkaline leaching process, under the dual effect of RMES decomposition and selective microwave heating, the surface of the nonporous RMES particles exhibited a morphology comprising slits or holes; the surfaces of the particles were loose and porous, which played a crucial role in improving the conversion efficiency of the fluorinated REEs. Under the optimal reaction conditions—reaction temperature of 150 °C, initial NaOH concentration of 60 %, NaOH-to-slag mass ratio of 4:1, microwave power of 700 W, reaction time of 120 min, and stirring speed of 300 r/min—the conversion rate of fluorinated REEs reached 99.17 %.

(2) A leaching kinetics study showed that the conversion of fluorinated REEs was dependent on the chemical reaction rate at the particle surface. The apparent activation energy of the microwave-assisted atmospheric alkaline leaching process was calculated to be 12.458 kJ/mol lower than that of conventional leaching. The kinetic equation of the microwave-assisted atmospheric alkaline leaching process is $1-(1-X)^{1/3} = 56.38[NaOH]^{2.796}[M_{RMES}/M_{NaOH}]^{1.6727}[P]^{0.4477}[S]^{0.7208}e^{-54872t/RT}$.

Data availability statement

Sharing research data helps other researchers in their subsequent studies, and we are willing to make our data publicly available upon request.

Ethics declarations

Review and/or approval by an ethics committee was not needed for this study because there are no moral and ethical issues involved in this study, the research of this thesis is an experimental study on the recovery of valuable metal elements from solid wastes to provide technical and theoretical safeguards for environmental protection and secondary resource recycling.

CRediT authorship contribution statement

Yusufujiang Mubula: Writing – review & editing, Writing – original draft, Resources, Methodology, Investigation, Funding acquisition, Formal analysis, Conceptualization. **Mingming Yu:** Writing – review & editing, Supervision, Funding acquisition. **Delong Yang:** Writing – original draft, Data curation. **Heyue Niu:** Software, Data curation. **Hongju Gu:** Software, Data curation. **Tingsheng Qiu:** Writing – review & editing, Supervision. **Guangjun Mei:** Writing – review & editing, Supervision.

Declaration of competing interest

The authors declare the following financial interests/personal relationships which may be considered as potential competing interests:

Yu Mingming reports financial support was provided by the Natural Science Foundation of the Jiangxi Province. Yu Mingming reports financial support was provided by the Young Elite Scientists Sponsorship Program by CAST (2022QNRC001). Yusufujiang Mubula reports financial support was provided by the Ganzhou City science and technology innovation talent project (2023CYZ26999). Yusufujiang Mubula reports financial support was provided by the Jiangxi Province Graduate Student Innovation Special Fund Project (YC2023–S642). Yu Mingming reports financial support was provided by the Open Project of Guangxi Key Laboratory of Nonferrous Metals and Characteristic Materials Processing (2022GXYSOF11). If there are other authors, they declare that they have no known competing financial interests or personal relationships that could have appeared to influence the work reported in this paper.

Acknowledgements

This work was mainly funded by the Natural ScienceFoundation of the Jiangxi Province (20224BAB204038), the Young Elite Scientists Sponsorship Program by CAST (2022QNRC001), the Ganzhou City science and technology innovation talent project (2023CYZ26999), the Jiangxi Province Graduate Student Innovation Special Fund Project (YC2023–S642), and the Open Project of Guangxi Key Laboratory of Nonferrous Metals and Characteristic Materials Processing (2022GXYSOF11).

References

[1] H. Zhu, Rare earth metal production by molten salt electrolysis, Encyclopedia of Applied Electrochemistry (2014) 1765–1772, https://doi.org/10.1007/978-1-4419-6996-5455.
[2] R.J. Reash, Energy and the environment: striking a balance, Integrated Environ. Assess. Manag. 17 (5) (2021 Sep) 899–900, https://doi.org/10.1002/ieam.4477.
[3] Y. Yang, T. Wei, M. Xiao, F. Niu, L. Shen, Rare earth recovery from fluoride molten-salt electrolytic slag by borax roasting-hydrochloric acid leaching, Jom 72 (2) (2020) 939–945, https://doi.org/10.1007/s11837-019-03732-0.
[4] K.Z.K. Zhao, Y.W.Y. Wang, N.F.N. Feng, Preparation of Al-Ti master alloy by electrochemical recovery of titanium-reducing slag in molten salts, J. Miner. Met. Mater. Soc.: J. Miner. Met. Mater. Soc. 70 (5) (2018) 758–763, https://doi.org/10.1016/j.jos.2021.05.001.
[5] A. Kumari, Randhawa NS. Dipali, S.K. Sahu, Electrochemical treatment of spent NdFeB magnet in organic acid for recovery of rare earths and other metal values, J. Clean. Prod. 309 (1) (2021) 127393, https://doi.org/10.1016/j.jclepro.2021.127393.
[6] Y.L.Y. Liang, Y.L.Y. Li, L.X.L. Xue, Y.Z.Y. Zou, Extraction of rare earth elements from fluoride molten salt electrolytic slag by mineral phase reconstruction, J. Clean. Prod. 177 (3) (2018) 567–572, https://doi.org/10.1016/j.jclepro.2017.12.244.
[7] L. Tian, L. Chen, A. Gong, X. Wu, C. Cao, Z. Xu, Recovery of rare earths, lithium and fluorine from rare earth molten salt electrolytic slag via fluoride sulfate conversion and mineral phase reconstruction, Miner. Eng. 170 (8) (2021) 106965, https://doi.org/10.1016/j.mineng.2021.106965.
[8] Y. Yang, L. Li, M. Xiao, F. Niu, Transformation mechanism and leaching performance of rare earth fluoride molten salt slag in the process of Na2CO3-roasting, Zhongnan Daxue Xuebao (Ziran Kexue Ban)/Journal of Central South University (Science and Technology) 50 (5) (2019) 1035–1041, https://doi.org/10.11817/j.issn.16727207.2019.05.004.
[9] Y. Mubula, M. Yu, D. Yang, B. Lin, Y. Guo, T. Qiu, Recovery of valuable elements from solid waste with the aid of external electric field: a review, J. Environ. Chem. Eng. 11 (6) (2023) 111237, https://doi.org/10.1016/j.jece.2023.111237.
[10] H.Q. Peng, Formation cause, composition analysis and comprehensive utilization of rare earth solid wastes, J. Rare Earths 27 (6) (2009) 1096–1102, https://doi.org/10.1016/S1002-0721(08)60394-4.
[11] Z. Tong, X. Hu, H. Wen, Effect of roasting activation of rare earth molten salt slag on extraction of rare earth, lithium and fluorine, J. Rare Earths 41 (2) (2022) 300–308, https://doi.org/10.1016/j.jre.2022.02.014.
[12] H. Wu, H. Yan, Rare earth recovery from fluoride molten-salt electrolytic slag by sodium carbonate roasting-hydrochloric acid leaching, J. Rare Earths 41 (8) (2022) 1242–1249, https://doi.org/10.1016/j.jre.2022.07.001.
[13] Y. Lai, J. Li, S. Zhu, K. Liu, Q. Xia, M. Huang, et al., Recovery of rare earths, lithium, and fluorine from rare earth molten salt electrolytic slag by mineral phase reconstruction combined with vacuum distillation, Separ. Purif. Technol. 310 (1) (2023) 123105, https://doi.org/10.1016/j.seppur.2023.123105.
[14] H. Hu, J. Wang, Selective extraction of rare earths and lithium from rare earth fluoride molten-salt electrolytic slag by nitration, Hydrometallurgy 200 (1) (2021) 105552, https://doi.org/10.1016/j.hydromet.2021.105552.
[15] J. Wang, H. Hu, Selective extraction of rare earths and lithium from rare earth fluoride molten-salt electrolytic slag by sulfation, Miner. Eng. 160 (1) (2021) 106711, https://doi.org/10.1016/j.mineng.2020.106711.
[16] D. Yang, M. Yu, Y. Mubula, W. Yuan, Z. Huang, B. Lin, et al., Recovering rare earths, lithium and fluorine from rare earth molten salt electrolytic slag using sub-molten salt method, J. Rare Earths (2023), https://doi.org/10.1016/j.jre.2023.08.009.

[17] C.L.C. Liu, S.J.S.H. Ju, L.Z.L.B. Zhang, C.S.C. Srinivasakannan, J.P.J.H. Peng, T.L.T.Q. Le, et al., Recovery of valuable metals from jarosite by sulphuric acid roasting using microwave and water leaching, Can. Metall. Q. 56 (1) (2017) 1–9, https://doi.org/10.1080/00084433.2016.1242972.
[18] E.R. Bobicki, Q. Liu, Z. Xu, Microwave heating of ultramafic nickel ores and mineralogical effects, Miner. Eng. 58 (1) (2014) 22–25, https://doi.org/10.1016/j.mineng.2014.01.003.
[19] P.R.P.M. Reddy, Y.H.Y. Huang, C.C.C. Chen, P.C.P. Chang, Y.H.Y. Ho, Evaluating the potential nonthermal microwave effects of microwave-assisted proteolytic reactions, J. Proteonomics 80 (27) (2013) 160–170, https://doi.org/10.1016/j.jprot.2013.01.005.
[20] L.H.L. Hu, Y.W.Y. Wang, B.L.B. Li, D.D.D. Du, J.X.J.H. Xu, Diastereoselectivity in the Staudinger reaction: a useful probe for investigation of nonthermal microwave effects, Tetrahedron 63 (38) (2008) 9387–9392, https://doi.org/10.1016/j.tet.2007.06.112.
[21] T. Wen, Y. Zhao, Q. Ma, Q. Xiao, T. Zhang, J. Chen, et al., Microwave improving copper extraction from chalcopyrite through modifying the surface structure, J. Mater. Res. Technol. 9 (1) (2020) 263–270, https://doi.org/10.1016/j.jmrt.2019.10.054.
[22] T.W.T. Wen, Y.Z.Y. Zhao, Q.X.Q. Xiao, Q.M.Q. Ma, S.K.S. Kang, H.L.H. Li, et al., Effect of microwave-assisted heating on chalcopyrite leaching of kinetics, interface temperature and surface energy, Results Phys. 7 (1) (2017) 2594–2600, https://doi.org/10.1016/j.rinp.2017.07.035.
[23] T. Abo Atia, J. Spooren, Fast microwave leaching of platinum, rhodium and cerium from spent non-milled autocatalyst monolith, Chem. Eng. Process 164 (1) (2021) 108378, https://doi.org/10.1016/j.cep.2021.108378.
[24] M. Laubertova, T. Havlik, L. Parilak, B. Derin, J. Trpcevska, The effects of microwave-assisted leaching on the treatment of electric ARC furnace dusts, Arch. Metall. Mater. 65 (1) (2020) 321–328, https://doi.org/10.24425/amm.2020.131733.
[25] J.W.J. Wang, Y.Z.Y. Zhang, J.H.J. Huang, T.L.T. Liu, Kinetic and mechanism study of vanadium acid leaching from black shale using microwave heating method, J. Miner. Met. Mater. Soc.: J. Miner. Met. Mater. Soc. 70 (6) (2018) 1031–1036, https://doi.org/10.1007/s11837-018-2859-3.
[26] Y.K. Huang, Z.Y.A, L.J, Decomposition of the mixed rare earth concentrate by microwave-assisted method, J. Rare Earths 34 (5) (2016) 529–535, https://doi.org/10.1016/S1002-0721(16)60058-3.
[27] Q. Ye, H.Z.H. Zhu, L.Z.L. Zhang, P.L.P. Liu, G.C.G. Chen, J.P.J. Peng, Carbothermal reduction of low-grade pyrolusite by microwave heating, RSC Adv. 4 (102) (2014) 58164–58170, https://doi.org/10.1039/C4RA08010F.
[28] W. Ma, C. Tao, H. Li, Z. Liu, R. Liu, Dynamics analysis of extraction of manganese intensified by electric field, Materials science, energy technology and power engineering II (MEP2018) (1) (2018) 40037, https://doi.org/10.1063/1.5041179, 1971.
[29] Z.Y.Z. Yang, H.L.H. Li, X.Y.X. Yin, Z.Y.Z. Yan, X.Y.X. Yan, B.X.B. Xie, Leaching kinetics of calcification roasted vanadium slag with high CaO content by sulfuric acid, Int. J. Miner. Process. 133 (10) (2014) 105–111, https://doi.org/10.1016/j.minpro.2014.10.011.
[30] E. Kavcı, T. Çalban, S. Çolak, S.K.H.C. Kuşlu, Leaching kinetics of ulexite in sodium hydrogen sulphate solutions, J. Ind. Eng. Chem. 20 (5) (2014) 2625–2631, https://doi.org/10.1016/j.jiec.2013.12.089.
[31] X. Zhu, W. Li, X. Guan, Kinetics of titanium leaching with citric acid in sulfuric acid from red mud, Trans. Nonferrous Metals Soc. China 25 (9) (2015) 3139–3145, https://doi.org/10.1016/S1003-6326(15)63944-9.